nature microbiology

LETTERS

https://doi.org/10.1038/s41564-018-0271-y

A *Chlamydia* effector combining deubiquitination and acetylation activities induces Golgi fragmentation

Jonathan N. Pruneda[1], Robert J. Bastidas[2,5], Erithelgi Bertsoulaki[3,5], Kirby N. Swatek[1], Balaji Santhanam[4], Michael J. Clague[3], Raphael H. Valdivia[2], Sylvie Urbé[3] and David Komander[1*]

Pathogenic bacteria are armed with potent effector proteins that subvert host signalling processes during infection[1]. The activities of bacterial effectors and their associated roles within the host cell are often poorly understood, particularly for *Chlamydia trachomatis*[2], a World Health Organization designated neglected disease pathogen. We identify and explain remarkable dual Lys63-deubiquitinase (DUB) and Lys-acetyltransferase activities in the *Chlamydia* effector ChlaDUB1. Crystal structures capturing intermediate stages of each reaction reveal how the same catalytic centre of ChlaDUB1 can facilitate such distinct processes, and enable the generation of mutations that uncouple the two activities. Targeted *Chlamydia* mutant strains allow us to link the DUB activity of ChlaDUB1 and the related, dedicated DUB ChlaDUB2 to fragmentation of the host Golgi apparatus, a key process in *Chlamydia* infection for which effectors have remained elusive. Our work illustrates the incredible versatility of bacterial effector proteins, and provides important insights towards understanding *Chlamydia* pathogenesis.

During infection, many Gram-negative pathogenic bacteria translocate effector proteins directly into host cells to modify signalling pathways important for invasion, survival and replication. One particularly interesting family of effectors are those belonging to the CE-clan of cysteine proteases. Members of this family have variously been found to be proteases for ubiquitin-like (Ubl) modifiers, DUBs or even Ser/Thr acetyltransferases (AcTs)[3–11], which is striking considering that they all share a structurally similar Cys protease fold. Physiologically, the activities are used against host inflammatory pathways. Deubiquitinases in particular are used by a wide range of pathogens to switch off ubiquitin (Ub)-dependent inflammatory signalling processes[12], or interfere with microbe-directed autophagy (xenophagy) pathways. CE family DUBs, such as *Legionella* SidE, *Salmonella* SseL and *Chlamydia* ChlaDUB1, have been shown to mediate inhibition of autophagy, NF-κB signalling and cell death during infection[10,13–15]. Similarly, the AcT activities of *Yersinia* YopJ and *Salmonella* AvrA modify phosphorylation sites, and directly block mitogen-activated protein kinase activation required for inflammatory signalling and innate immunity[7–9].

Recent phylogenetic analyses and crystal structures have started to explain the seemingly disconnected catalytic activities among CE family members, but the conundrum of the identical catalytic fold has remained intriguing. Indeed, a direct biochemical comparison of DUB and AcT activities in CE family proteins has not yet been performed. We used our panel of purified bacterial CE enzymes from a range of pathogens alongside their catalytically inactive variants (Fig. 1a) to test for DUB activity by monitoring cleavage of K63-linked diubiquitin (diUb) (Fig. 1b). In parallel, we tested for AcT activity by monitoring auto-acetylation via radioisotope incorporation following incubation with ^{14}C Acetyl-Coenzyme A (Fig. 1c). This analysis revealed *Salmonella* SseL, *Escherichia* ElaD, *Shigella* ShiCE, and *Rickettsia* RickCE to be dedicated DUBs, and identified *Legionella* LegCE, *Yersinia* YopJ, and *Salmonella* AvrA as dedicated AcTs.

Remarkably, *Chlamydia* ChlaDUB1 could perform both DUB and AcT reactions, seemingly using the same catalytic Cys residue (compare Fig. 1b,c). ChlaDUB1 is phylogenetically distinct from the YopJ-like family[11], but showed similar rates of auto-acetylation compared with YopJ and AvrA (although YopJ acetylation of its substrate MEK2 (ref. [8]) is markedly faster, see Supplementary Fig. 1a–c). Importantly, ChlaDUB1 auto-acetylation occurs at Lys residues (Supplementary Fig. 1d,e), whereas YopJ-like family members predominantly target Ser/Thr residues[7–9]. Furthermore, ChlaDUB1 AcT activity is not regulated by phytic acid (inositol hexakisphosphate, IP6) (Supplementary Fig. 1f,g), in contrast to YopJ-like enzymes[16,17]. This identified ChlaDUB1 as a bona fide Lys-AcT in addition to being a Lys63-specific DUB.

To explain how ChlaDUB1 could perform two seemingly disparate chemical reactions, namely deubiquitination—a hydrolysis reaction, and acetylation—a condensation reaction, we determined crystal structures of the enzyme bound to Ub, and bound to Coenzyme A (CoA) at 1.9 Å and 2.1 Å resolution, respectively (Fig. 1d and Supplementary Table 1). The structures showed hardly any conformational changes between each other, or in comparison with previous apo structures (pdb id 5HAG[11], 5B5Q[15]) with overall root mean squared deviations < 1 Å (Fig. 1d and Supplementary Fig. 2a), but revealed distinct binding sites for Ub and CoA.

The ChlaDUB1~Ub structure (Supplementary Fig. 2b) was obtained using the Ub activity-based probe Ub-propargylamide (Ub-PA), which covalently links one Ub molecule into the enzymatic S1 site (Supplementary Fig. 3). ChlaDUB1 forms similar interactions with Ub compared with other CE proteases[10,11,18–20], involving both the Ile44 and Ile36 hydrophobic patches of Ub (Supplementary Fig. 2c,d).

[1]Division of Protein and Nucleic Acid Chemistry, MRC Laboratory of Molecular Biology, Cambridge, UK. [2]Department of Molecular Genetics and Microbiology, Duke University, Durham, NC, USA. [3]Cellular and Molecular Physiology, Institute of Translational Medicine, University of Liverpool, Liverpool, UK. [4]Division of Structural Studies, MRC Laboratory of Molecular Biology, Cambridge, UK. [5]These authors contributed equally: Robert J. Bastidas, Erithelgi Bertsoulaki. *e-mail: dk@mrc-lmb.cam.ac.uk

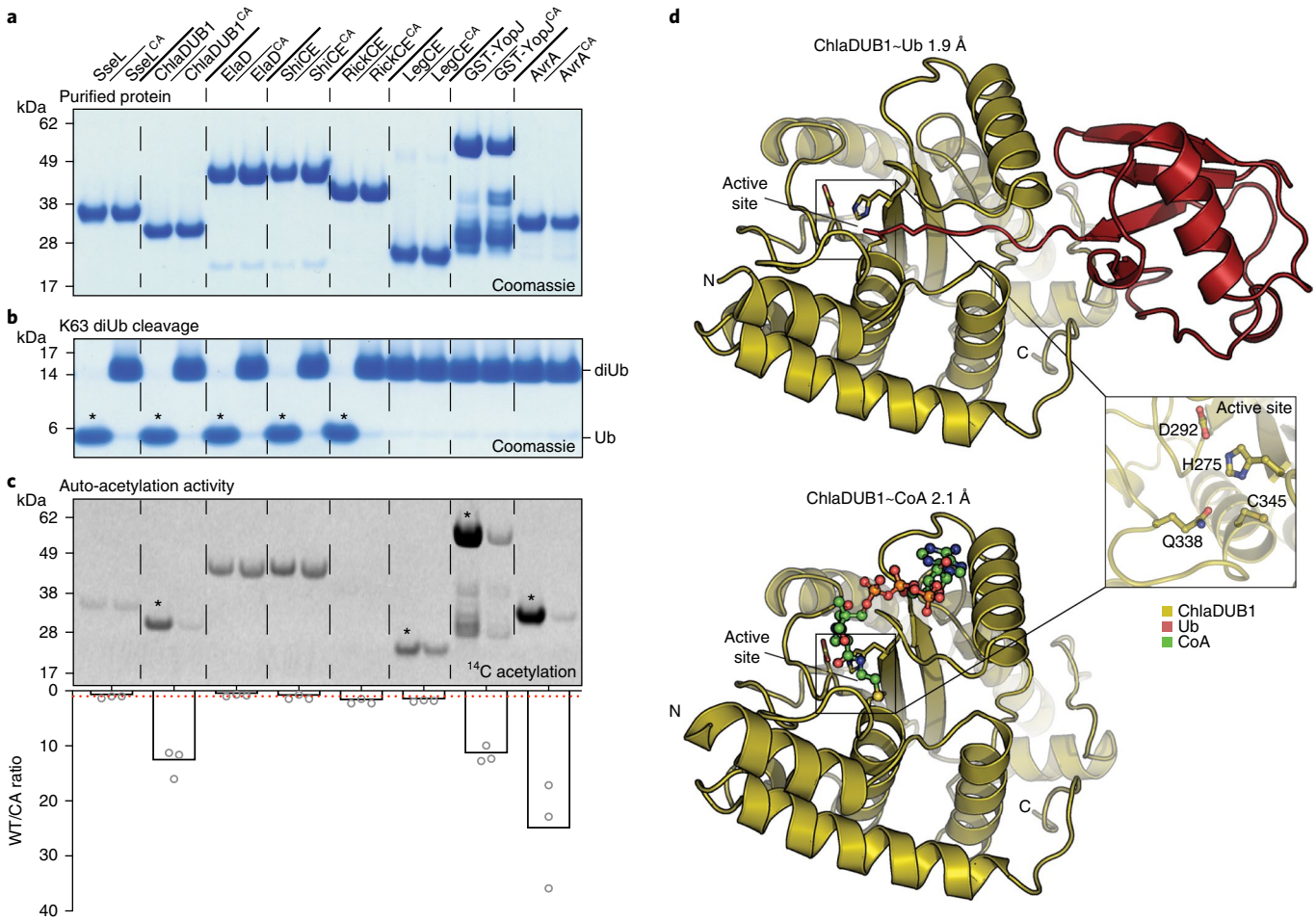

Fig. 1 | Identification of specialized and dual-function CE-clan enzymes. a, Panel of purified bacterial CE-clan enzymes and their catalytically inactive Cys-to-Ala mutants. **b**, Deubiquitinase assay monitoring cleavage of K63-linked diUb following overnight incubation. **c**, Acetyltransferase assay monitoring ^{14}C incorporation following a 2 h incubation of each protein with ^{14}C-labelled Acetyl-CoA. Below, histogram representation of the wild-type/inactive Cys-to-Ala (WT/CA) ^{14}C incorporation ratio following normalization of the ^{14}C autoradiography signal to the Coomassie stain. The average of three replicated experiments is plotted. A WT/CA ratio of one indicates no AcT activity, and is denoted by a red dashed line. Gels in **a, b** and **c** are representative of triplicate experiments. All uncropped gels are shown in Supplementary Fig. 10. Asterisks indicate appreciable DUB (**b**) or AcT (**c**) activity. **d**, ChlaDUB1 complex crystal structures that capture intermediate stages of deubiquitinase (top) and acetyltransferase (bottom) activities. Inset, a representative view of the ChlaDUB1 active site showing the Cys-His-Asp catalytic triad and the Gln oxyanion hole.

The ChlaDUB1~CoA structure (Supplementary Fig. 2e) revealed a disulfide bridge between the cofactor's cysteamine and the catalytic Cys, and identified a charge-complementary binding site for CoA near the active site (Supplementary Fig. 2f). The ChlaDUB1 CoA-binding site is distinct from the CoA-binding sites of the YopJ-like effector HopZ1a[16] and arylamine N-acetyltransferases (NATs)[21] (Supplementary Fig. 2g,h), and is also removed from the Ub-binding site (Supplementary Fig. 3).

Both structures together reveal the importance of an inserted helix that is unique to ChlaDUB1 and not present in other CE enzymes from bacteria, viruses or eukaryotes; we had previously annotated this element as Variable Region 3 (VR-3)[11]. One face of this VR-3 helix contacts the adenosine and phosphate groups of the CoA molecule (Fig. 2a,b). Remarkably, the opposite face of the VR-3 helix binds the Ile36-patch of Ub (Fig. 2a,b and Supplementary Fig. 2i). This arrangement enables both DUB and AcT activities to utilize the same active site (Fig. 1d and Supplementary Fig. 4a,b), via spatially separated, independent binding sites for Ub and CoA. Consistently, Ub compromises AcT activity, but when the Ub C-terminus is missing, auto-acetylation is restored (Supplementary Fig. 4c). Separate binding sites for Ub and CoA further enabled us to uncouple DUB and AcT activity. ChlaDUB1 AcT activity was strongly diminished by mutation of K268E (VR-3), or G272E without affecting DUB activity. In contrast, DUB activity was abrogated by I267R (VR-3) or I225A mutation, yet these mutants did not affect auto-acetylation (Fig. 2a,c and Supplementary Fig. 5a).

The VR-3 helix is central to dual activities in *C. trachomatis* (*C.t.*) ChlaDUB1 and present in all *Chlamydia* ChlaDUB homologues, such as ChlaDUB of *C. abortus* (*C.a.*), a cattle pathogen that is transmissible to humans. A 1.5 Å crystal structure of *C.a.* ChlaDUB confirmed the register of the predicted VR-3 helix as shown in the sequence alignment (Fig. 2d, Supplementary Fig. 5d,e and Supplementary Table 1). Importantly, the Ub- and CoA-coordinating residues within VR-3 are not jointly conserved (Fig. 2d), and we hypothesized that *C.t.* ChlaDUB2 should be a dedicated DUB, while *C.a.* ChlaDUB should be a dedicated AcT. Indeed, these predictions could be confirmed biochemically (Fig. 2e,f and Supplementary Fig. 5b,c). Together, our data strongly suggested that *Chlamydia* species evolved ChlaDUB effectors with dual activities and potentially multiple functions.

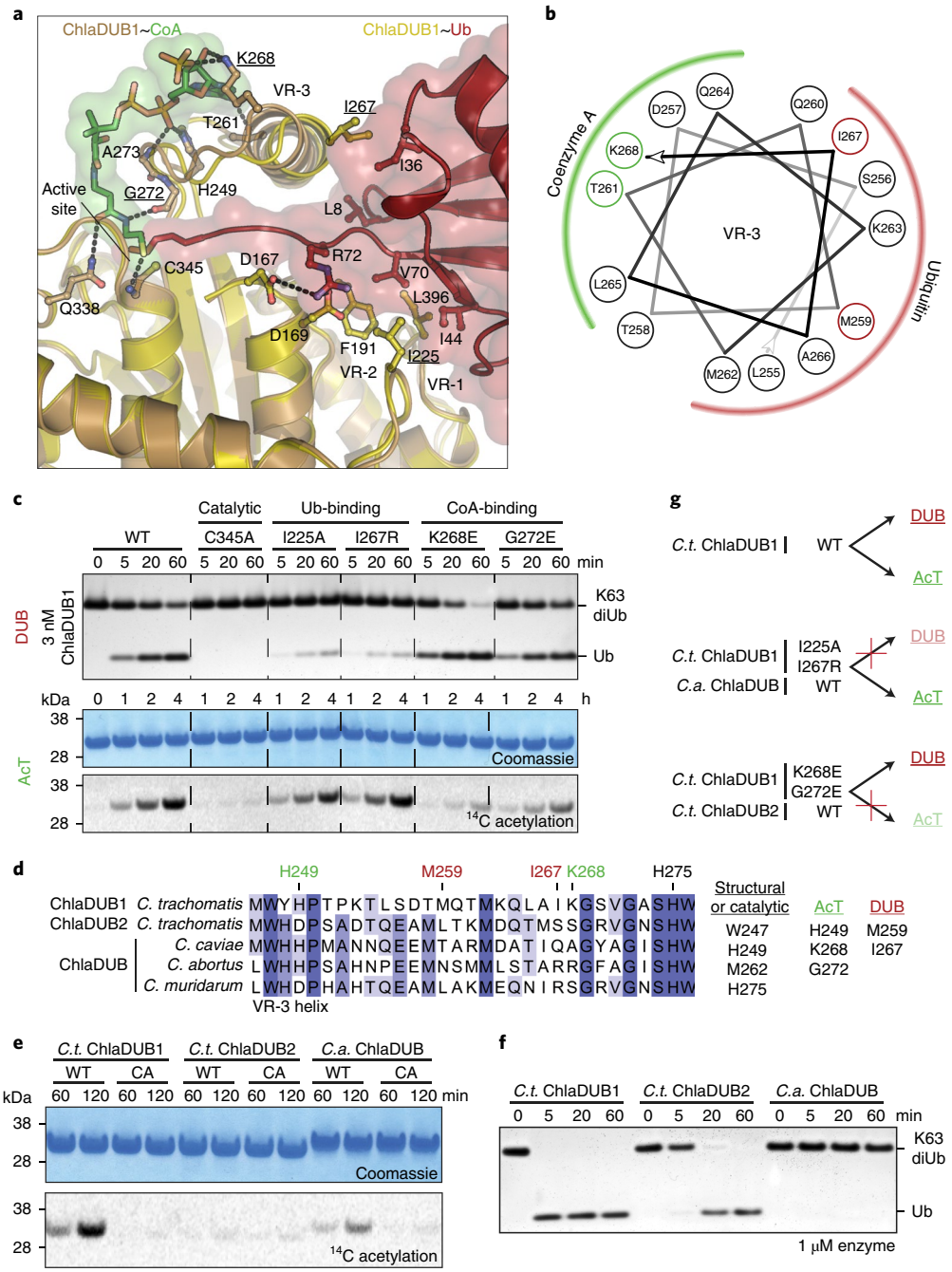

Fig. 2 | Molecular dissection of dual deubiquitinase/acetyltransferase activities. a, Close-up of the ChlaDUB1:CoA (brown:green) and ChlaDUB1:Ub (tan:red) interfaces with key interacting residues shown in ball-and-stick. Hydrogen bonds are shown as dashed lines. **b**, Helical wheel diagram illustrating the amphipathic nature of the ChlaDUB1 VR-3 helix, and its interactions with Ub or CoA (coloured in red and green, respectively). **c**, Deubiquitinase (top) and acetyltransferase (bottom) assays illustrating that while both activities require the catalytic Cys residue, mutations in the Ub-binding and CoA-binding regions separate the two functions. A representative gel is shown of triplicate experiments. **d**, Sequence alignment of the VR-3 helix for orthologous *Chlamydia* ChlaDUB enzymes. The catalytic His, CoA-binding (green) and Ub-binding (red) residues are marked, and additional contacts are listed. **e**, ^{14}C acetylation assay with the ChlaDUB orthologues from *C. trachomatis* (*C.t.* ChlaDUB2) and *C. abortus* (*C.a.* ChlaDUB). **f**, Deubiquitinase assay monitoring K63-linked diUb cleavage by the *Chlamydia* ChlaDUB orthologues. Gels in **e** and **f** are representative of triplicate experiments. All uncropped gels are shown in Supplementary Fig. 10. **g**, Schematic depicting how DUB and AcT functions can be separated either by structure-guided mutation or evolution as represented by the ChlaDUB orthologues.

Functional characterization of *Chlamydia* effectors has remained challenging, mostly due to the rudimentary tools available for genetic manipulation of *Chlamydia*[22]. Nonetheless, we set out to uncover roles for the DUB/AcT ChlaDUB1 and the dedicated DUB ChlaDUB2 utilizing mutant strains harbouring catalytically inactive ChlaDUB1 and ChlaDUB2 variants. One strain, containing a mutation leading to an amino acid substitution in the ChlaDUB2 catalytic His residue (H203Y) that inactivates the enzyme (Supplementary Fig. 6a), was identified from a collection of chemically mutagenized *C. trachomatis* strains[23]. This strain was back-crossed to wild-type

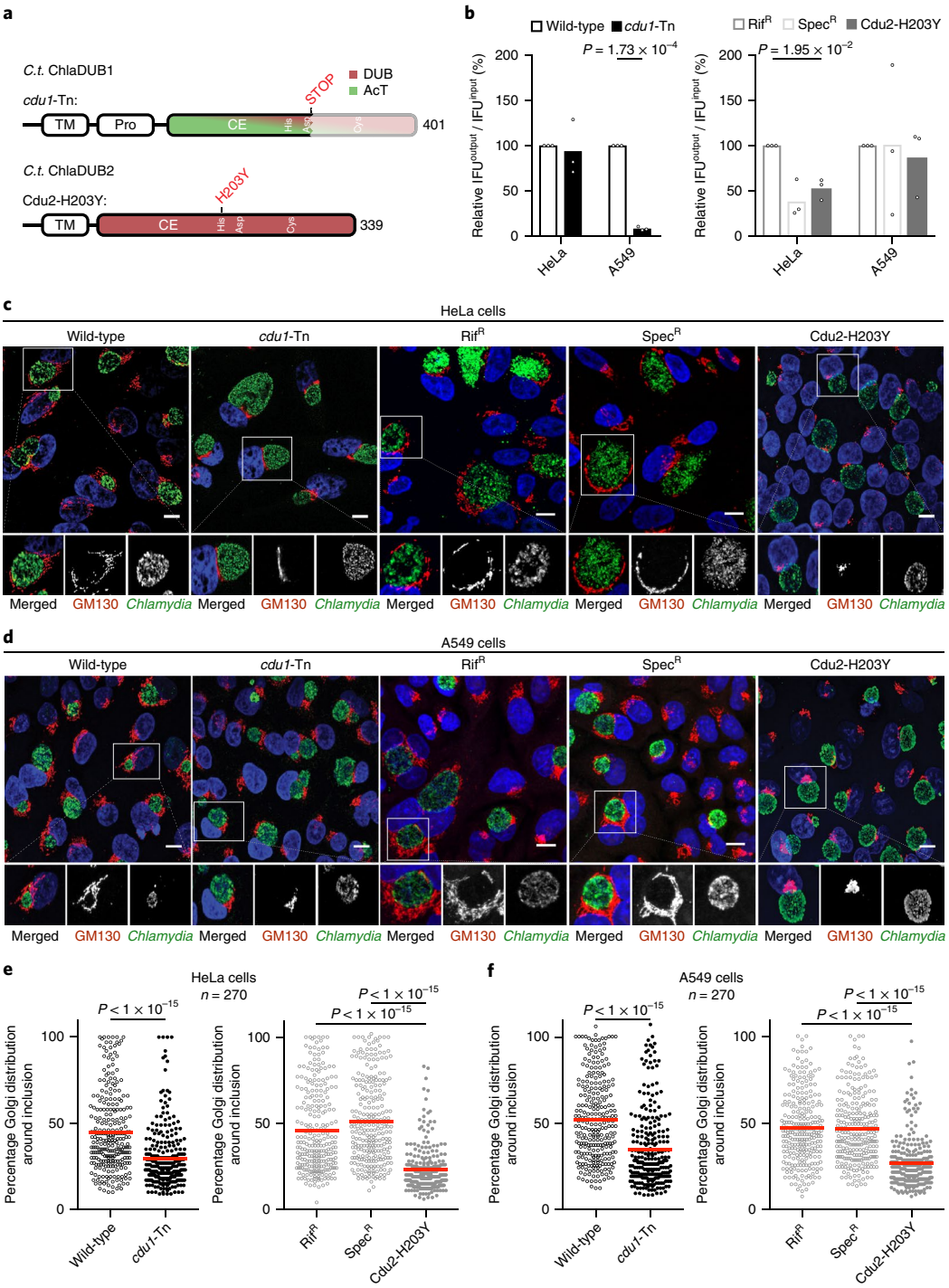

Fig. 3 | ChlaDUB function is required for *C. trachomatis* Golgi fragmentation. a, Topology diagram illustrating *C.t.* ChlaDUB1 and *C.t.* ChlaDUB2 domain architecture, with active site residues annotated within the catalytic domains. Changes present in the *cdu1*-Tn and Cdu2-H203Y defective strains are shown above. **b**, *C. trachomatis* growth assay measured as inclusion forming units (IFU) output per IFU input following a 48 h infection in either HeLa or A549 cells. Values were normalized to 100% for wild-type. The statistical significance of parental controls was measured using a two-tailed Welch's *t*-test. HeLa: wild-type–*cdu1*-Tn, $P = 0.768$; Rif^R–Cdu2-H203Y, $P = 0.0195$; Spec^R–Cdu2-H203Y, $P = 0.392$. A549: wild-type–*cdu1*-Tn, $P = 0.000173$; Rif^R–Cdu2-H203Y, $P = 0.615$; Spec^R–Cdu2-H203Y, $P = 0.791$. $n = 3$. **c**, Representative confocal images showing Golgi fragmentation and redistribution around the *Chlamydia* inclusion following a 26 h infection of HeLa cells. Samples were immunostained with anti-GM130 (cis-Golgi, red) and anti-Slc1 (*Chlamydia*, green) antibodies, and Hoechst stained (DNA, blue). Isolated channels for the boxed region are shown below, and full versions are shown in Supplementary Fig. 6b. Scale bars, 10 μm. **d**, As in **c** for A549 cells. Full versions are shown in Supplementary Fig. 6c. **e**, Quantification of **c** following measurement of Golgi distribution around the circumference of the *Chlamydia* inclusion in 90 cells for each of three independent replicates. Mean values are shown as a red bar with individual data points overlaid. Statistical significance compared with parental was measured using a two-tailed Mann–Whitney *U*-test. Wild-type–*cdu1*-Tn, $P < 1 \times 10^{-15}$; Rif^R–Cdu2-H203Y, $P < 1 \times 10^{-15}$; Spec^R–Cdu2-H203Y, $P < 1 \times 10^{-15}$. Separated plots for each replicate are shown in Supplementary Fig. 6d. **f**, As in **e** for A549 cells. Wild-type–*cdu1*-Tn, $P < 1 \times 10^{-15}$; Rif^R–Cdu2-H203Y, $P < 1 \times 10^{-15}$; Spec^R–Cdu2-H203Y, $P < 1 \times 10^{-15}$. Separated plots for each replicate are shown in Supplementary Fig. 6e.

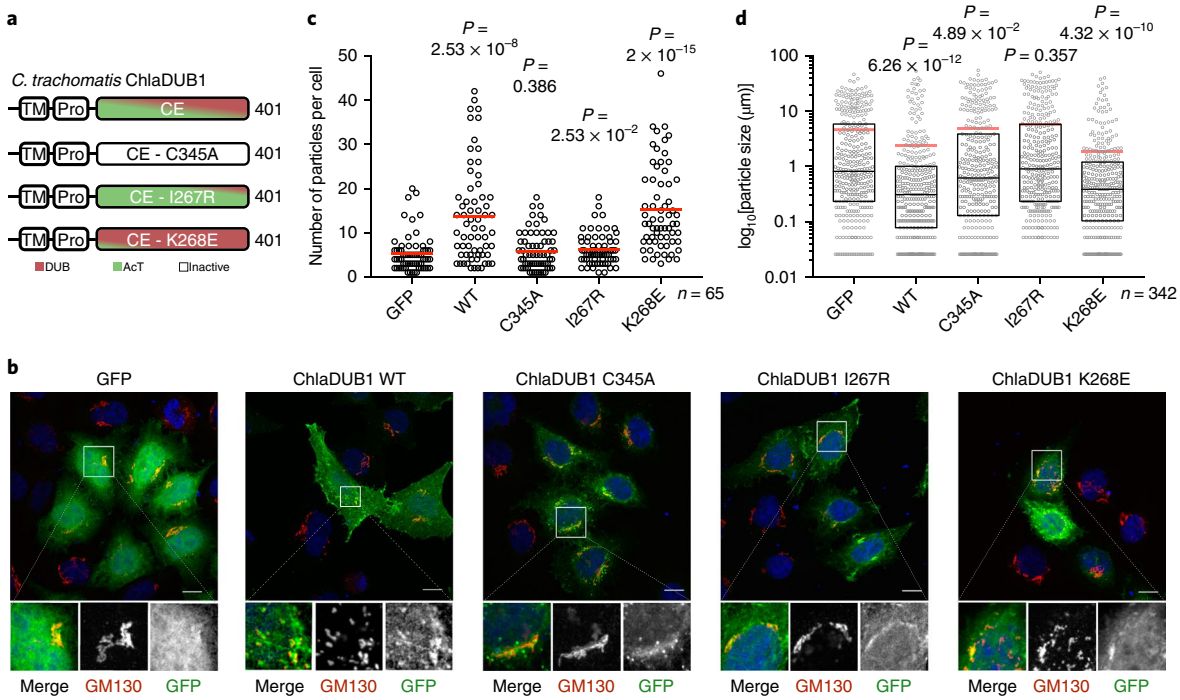

Fig. 4 | ChlaDUB deubiquitinase activity is responsible for *C. trachomatis* Golgi fragmentation. a, Topology diagram illustrating the constructs used to characterize activity dependence of Golgi fragmentation following expression of ChlaDUB1 in mammalian cells. Separation-of-function mutations were selected from structural and biochemical work discussed in Fig. 2. **b**, Representative confocal images showing Golgi fragmentation in HeLa cells following expression of GFP-tagged ChlaDUB1. Samples were immunostained with anti-GM130 (cis-Golgi, red) and DAPI stained (DNA, blue). GFP fluorescence is shown in green. Isolated channels for the boxed region are shown below, and full versions are shown in Supplementary Fig. 7b. Scale bars, 10 μm. **c**, Quantification of cis-Golgi-stained puncta from **b** for ~65 cells in each of three independent replicates (two remaining replicates are plotted in Supplementary Fig. 7c). Mean values are shown as red bars with individual data points overlaid. Statistical significance compared with GFP control was measured using a two-tailed Mann–Whitney *U*-test. GFP-WT, $P = 2.53 \times 10^{-8}$; GFP-C345A, $P = 0.386$; GFP-I267R, $P = 0.0253$; GFP-K268E, $P = 2 \times 10^{-15}$. **d**, Measurement of cis-Golgi-stained puncta size from **b** for ~65 cells in each of three independent replicates (two remaining replicates are plotted in Supplementary Fig. 7d). Mean values are shown as red bars, median values are shown as black bars inside a quartile box plot, with individual data points overlaid. Statistical significance compared with GFP control was measured using a two-tailed Mann–Whitney *U*-test. GFP-WT, $P = 6.26 \times 10^{-12}$; GFP-C345A, $P = 0.0489$; GFP-I267R, $P = 0.357$; GFP-K268E, $P = 4.32 \times 10^{-10}$.

C. trachomatis and a clean recombinant strain harbouring only the ChlaDUB2 H203Y variant was isolated (Cdu2-H203Y) (Fig. 3a and Supplementary Tables 2 and 3). For ChlaDUB1, we obtained a recently characterized ChlaDUB1 mutant strain[15] generated by transposon mutagenesis that introduced an early stop codon before the catalytic Cys residue (*cdu1*-Tn) (Fig. 3a and Supplementary Table 2).

The ChlaDUB1 and ChlaDUB2 loss of function strains left us in the privileged position of assessing the effects of either enzyme on host biology, and on contributions to *Chlamydia* infection. The *cdu1*-Tn mutant strain did not significantly reduce the number of infectious progeny in HeLa cells compared with a wild-type strain. This was markedly different in A549 cells, a human adenocarcinomic lung epithelial cell line, in which infection with the *cdu1*-Tn mutant strain reduced progeny by 90% (Fig. 3b). The latter was comparable to the effect of this strain in vivo using a transcervical mouse model of infection, whereas primary human fimbriae cells showed a bacterial growth defect only after prior stimulation with interferon-γ[15]. Surprisingly, the Cdu2-H203Y strain showed little to no growth defect in either HeLa or A549 cell lines compared with its two parental strains (see Methods) (Fig. 3b), suggesting that ChlaDUB1, with its additional AcT activity, may play a unique role in *Chlamydia* infection.

Next, we inspected infected cells by confocal microscopy. A prominent feature of *Chlamydia*-infected cells is the fragmentation and subsequent redistribution of the Golgi apparatus into ministacks that surround the pathogen-containing vacuole (termed the inclusion) at approximately 20 hours post infection[24,25]. Because ChlaDUB1 and ChlaDUB2 are actively expressed and secreted at this time post infection and have been shown to localize to the outside of the inclusion membrane where they could interact with neighbouring organelles[15,26], we used our *cdu1*-Tn and Cdu2-H203Y mutant strains to test for a contribution to Golgi redistribution following infection. Remarkably, at 26 hours post infection, both the *cdu1*-Tn and Cdu2-H203Y mutant strains showed a dramatic impairment in redistribution of the Golgi apparatus (Fig. 3c-f and Supplementary Fig. 6b–e). Since both ChlaDUB1 and ChlaDUB2 mutant strains affected host Golgi redistribution, this strongly suggested that DUB activity is required in this process. Moreover, the comparable individual impact of each mutant strain on Golgi redistribution (Fig. 3e,f) indicates either non-redundant roles for each DUB, or a strict dose dependency on DUB activity introduced by *Chlamydia* to invoke the observed cell biological effect. Finally, a similar extent of Golgi redistribution was seen in A549 but also HeLa cells, contrasting with the different impact of ChlaDUB mutant strains on bacterial growth rates (compare Fig. 3c–f with Fig. 3b). This lack of correlation had been observed previously in HeLa cells, for example with InaC that regulates Golgi redistribution without impacting the generation of bacterial progeny[23].

Our data suggested that ChlaDUB1 and ChlaDUB2 may have unrecognized roles in manipulating Golgi morphology and dynamics, which was corroborated in a simplified system (Fig. 4a).

Strikingly, we found that Golgi fragmentation was readily induced by sole expression of either ChlaDUB1 or ChlaDUB2 in HeLa cells (Fig. 4b, Supplementary Fig. 7a,b and Supplementary Fig. 8a,b). Expression of wild-type ChlaDUB1 and (to a lesser extent) ChlaDUB2 resulted in significant Golgi fragmentation as measured either by the number or the size of Golgi-stained puncta. Importantly, active site mutations eliminated this effect, which was again more pronounced for ChlaDUB1 (Fig. 4c,d, Supplementary Fig. 7c,d and Supplementary Fig. 8c,d). All ChlaDUB1 constructs showed an enriched localization to the Golgi apparatus, indicating that the introduced mutations exclusively affect activity (Fig. 4b and Supplementary Fig. 7b). ChlaDUB2 appeared to primarily localize to the endoplasmic reticulum (Supplementary Fig. 8e), which could explain its reduced ability to induce Golgi fragmentation compared with ChlaDUB1. Using our structure-guided mutations that separate ChlaDUB1 DUB and AcT functions (Figs. 2g and 4a), the Golgi fragmentation could be assigned as a DUB-dependent effect. A DUB-deficient I267R mutant was as defective in Golgi fragmentation as a catalytically inactive C345A construct, while an AcT-deficient ChlaDUB1 K268E mutant retained its Golgi fragmenting capabilities (Fig. 4b–d and Supplementary Fig. 7a–d).

This unveils a remarkable case of protein moonlighting[27], wherein a bacterial effector, *C. trachomatis* ChlaDUB1, performs two distinct enzymatic activities within its catalytic site, leading to separable cellular functions. Single amino acid substitutions can toggle between the activities, and this is used by closely related orthologues and paralogues in this enzyme family to modulate function (Fig. 2g). We further establish that the DUB activities present in ChlaDUB1, and also in the dedicated DUB paralogue ChlaDUB2, are necessary and sufficient for the fragmentation of the host Golgi apparatus, a prerequisite to Golgi redistribution around the *Chlamydia* inclusion. This adds ChlaDUB1 and ChlaDUB2 to the limited list of effectors and host factors implicated in this striking cell biological phenomenon[23–25,28,29] (see Supplementary Fig. 9). In overexpression studies, ChlaDUB1 has also been implicated with inhibition of NF-κB signalling[13] and cell death[15], and it is tempting to speculate that some of these effects are conferred by the AcT activity of ChlaDUB1. While this requires further study, the importance of ChlaDUB1 for *Chlamydia* infectivity[15] and its unique enzymatic nature make it an interesting candidate for future *Chlamydia*-targeted therapeutics.

Methods

Cloning and molecular biology. Generation of *Salmonella* Typhimurium SseL, *Chlamydia trachomatis* ChlaDUB1, *Escherichia coli* ElaD, *Shigella flexneri* ShiCE, *Rickettsia bellii* RickCE, *Legionella pneumophila* LegCE, *Yersinia pestis* YopJ, and *Salmonella* Typhimurium AvrA constructs have been described previously[11]. Sequences for *Chlamydia trachomatis* ChlaDUB2 and *Chlamydia abortus* ChlaDUB were obtained via gene synthesis (Life Technologies). Following amplification with KOD polymerase (EMD Millipore), the genes were inserted into the pOPIN-B or pOPIN-GFP vector[30] with the In-Fusion cloning method (Takara Bio USA). All mutagenesis was performed using the Quikchange method (Agilent).

Protein expression and purification. The expression and purification of SseL (24-340), ElaD (2-407), ShiCE (2-405), RickCE (378-691), LegCE (141-360), YopJ (1-288) and AvrA (1-288) has been described previously[11]. *C.t.* ChlaDUB1 (130-401), *C.t.* ChlaDUB2 (80-339) and *C.a.* ChlaDUB were expressed in *E. coli* Rosetta2 pLacI cells (Novagen) at 18 °C for 20 h following induction with 0.2 mM IPTG at an absorbance $A_{600\,nm}$ of 0.8–1.0. Cells were harvested in 25 mM Tris buffer (pH 7.4), 200 mM NaCl, 2 mM ß-mercaptoethanol (Buffer A) and subjected to one freeze–thaw cycle. EDTA-free Complete protease inhibitor tablets (Roche), DNase and Lysozyme were added prior to lysis by sonication. The resulting lysate was centrifuged at 35,000*g* for 25 min, and applied to Talon resin (Takara Bio USA). The resin was washed with Buffer A thoroughly prior to elution with Buffer A containing 250 mM imidazole. During overnight dialysis back to Buffer A at 4 °C, the His-tag was cleaved with His-3C protease. Following a reverse affinity step over regenerated Talon resin, the resulting protein was then concentrated (10,000 MWCO, EMD Millipore) and applied to a gel filtration column (Superdex75, GE Healthcare) equilibrated in 25 mM HEPES (pH 8.0), 150 mM NaCl, 5 mM DTT. Pure protein-containing fractions were concentrated, aliquoted and flash-frozen for storage at −80 °C.

Deubiquitinase assays. All enzymes were diluted to a '×2' concentration in 25 mM Tris (pH 7.4), 150 mM NaCl, 10 mM DTT and allowed to fully reduce for 20 min at room temperature. Then 6 µM diUb stocks were prepared in 100 mM Tris (pH 7.4), 100 mM NaCl, 10 mM DTT and mixed 1:1 with ×2 enzyme prior to incubation at 37 °C. Samples were quenched in reducing LDS sample buffer (ThermoFisher), resolved by SDS–PAGE, and visualized using silver stain (BioRad).

Ub/Ubl KG-TAMRA protease assays were performed as described previously[11].

Acetylation assays. All enzymes were diluted to 5 µM in 25 mM HEPES (pH 8.0), 50 mM NaCl, 0.5 mM DTT and incubated with 60 µM [1-^{14}C] Acetyl-CoA (60 mCi mmol^{-1}, PerkinElmer) at 37 °C for the indicated time. The panel shown in Fig. 1 and all subsequent assays with YopJ or AvrA additionally included 200 nM inositol hexakisphosphate (IP6). Reactions were quenched with reducing LDS sample buffer (ThermoFisher) and resolved by SDS–PAGE prior to staining with Coomassie. Gels were then dried and exposed to a Phosphor screen for several days prior to imaging on a Typhoon scanner (GE Healthcare). The ^{14}C autoradiography intensity was quantified using ImageJ[31] and normalized to the Coomassie stain signal.

Protein crystallization. The ChlaDUB1 (130–401)~Ub complex was purified by gel filtration following an overnight reaction at room temperature with 2-fold molar excess Ub-PA suicide probe[32]. Native ChlaDUB1~Ub crystals were obtained using protein prepared in 25 mM Tris (pH 7.4), 125 mM NaCl, 4 mM DTT and crystallized at 10 mg ml^{-1} in 0.1 M MES (pH 6.0), 20% PEG 6000, with a 400 nl sitting drop at 1:1 protein:precipitant ratio. SeMet ChlaDUB1~Ub crystals were obtained using protein at 7 mg ml^{-1} in 0.1 M HEPES (pH 7.1), 18% PEG 8 K, with a 200 nl sitting drop at 1:1 protein:precipitant ratio. The ChlaDUB1~CoA complex was crystallized by the addition of 2 mM CoA to 12 mg ml^{-1} ChlaDUB1, and mixing with 0.1 M HEPES (pH 7.2), 20% PEG 8000 at a 1:1 protein:precipitant ratio in a 400 nl sitting drop. *C. a.* ChlaDUB (108–377) was prepared in 25 mM HEPES (pH 8.0), 150 mM NaCl, 5 mM DTT and crystallized in 0.1 M Tris (pH 7.0), 0.2 M calcium acetate, 20% PEG 3000 with a 400 nl sitting drop at 1:1 protein:precipitant ratio. All crystals were cryoprotected with mother liquor containing 25% glycerol. Cryoprotectant for ChlaDUB1~CoA crystals also contained 5 mM CoA.

Data collection, structure determination and refinement. Data were collected at 100 K at the Diamond Light Source (DLS) beam lines I02, I03 and I04 (see Supplementary Table 1). Data collections were performed at 0.9798, 0.9795 and 0.9794 Å wavelengths for the ChlaDUB1~Ub, ChlaDUB1~CoA and *C.a.* ChlaDUB structures, respectively. Integration and scaling were performed using XDS[33] and Aimless[34], respectively. The ChlaDUB1~Ub structure was solved experimentally using a SeMet SAD dataset with PHENIX AutoSol and AutoBuild[35–37]. ChlaDUB1~CoA and *C.a.* ChlaDUB structures were solved using molecular replacement in Phaser[38] using the apo ChlaDUB1 structure (pdb id 5HAG). Iterative rounds of model building and refinement were performed using COOT[39] and PHENIX[35], respectively. Ramachandran statistics (favoured/allowed/outliers) for the ChlaDUB1~Ub, ChlaDUB1~CoA and *C.a.* ChlaDUB structures were 97.2/2.8/0, 97.4/2.6/0 and 98.0/2.0/0, respectively. All figures were generated using PyMOL (www.pymol.org).

Cell lines. HeLa, A549 and Vero cell lines were obtained from ATCC, where they were authenticated by morphology, karyotyping and short tandem repeat analyses. Stocks were routinely tested and confirmed negative for mycoplasma contamination.

***Chlamydia* growth conditions and infections.** HeLa, A549 and Vero cells were grown in high-glucose DMEM supplemented with L-glutamine, sodium pyruvate (Gibco, Life Technologies) and 10% FBS (Mediatech, CellGro), at 37 °C in a 5% CO_2 humidified incubator. All cells infected with *Chlamydia* were centrifuged at 3,500 r.p.m. for 30 min at 10 °C immediately on infection.

Chlamydia strains. All *Chlamydia* strains (Supplementary Table 2) were derived from *C. trachomatis* LGV biovar L2 434/Bu (wild-type). The *cdu1*-Tn strain was provided by Scott Hefty (University of Kansas) and is described previously[15]. The *cdu2-G607A* (Cdu2-H203Y) allele was identified in a collection of chemically mutagenized *C. trachomatis* L2 434/Bu strains by whole-genome sequencing of a collection of pooled mutant strains[23]. Strain CTL2M467 was identified as harbouring the *cdu2-G607A* single nucleotide variant (SNV) by Sanger sequencing of the *cdu2* (CTL0246) locus. Vero cells seeded in a 6-well plate were infected with CTL2M467. At 48 hours post infection (hpi), cell monolayers were lysed by hypotonic lysis, lysates sonicated, and bacterial cells collected by centrifugation at 14,000 r.p.m. for 15 min at 4 °C. Bacterial cell pellets were resuspended in 1X DNAse I buffer (New England Biolabs) and treated with 4 units of DNAse 1 (New England Biolabs) for 1 h at 37 °C to deplete co-purifying Vero DNA. Following a wash with PBS buffer, total DNA was isolated with a DNA isolation kit (DNeasy tissue and blood kit, Qiagen) following the manufacturer's instructions.

One µg of CTL2M467-enriched DNA was fragmented with NEBNext dsDNA Fragmentase (New England Biolabs) and DNA sequencing libraries prepared with a NEBnext DNA Library Prep Kit for Illumina according to the manufacturer's

instructions. Libraries were sequenced with the MiSeq DNA Sequencing Platform (Illumina, Inc.) at the Duke University IGSP sequencing facility. Genome assembly and SNV identification was performed with Geneious version 6 (Biomatters, http://www.geneious.com/). The *C. trachomatis* L2 434/Bu genome (GenBank no. NC_010287) was used as a reference sequence. All SNVs identified (Supplementary Table 3) were independently verified by Sanger sequencing. The strain M467 rs22 was isolated from a backcross of parental strain CTL2M467 (rifampin resistant-Rif^R) with a spectinomycin-resistant L2 434/Bu strain (Spec^R) as described previously[40]. Vero cells were co-infected with strains CTL2M467 (Rif^R) and L2 434/Bu (Spec^R) at a multiplicity of infection (m.o.i.) of 3 and a ratio of 1:1. At 48 hpi, crude cell lysates prepared in SPG buffer (0.25 M sucrose, 10 mM sodium phosphate, 5 nM glutamic acid) were used to infect Vero cells seeded in a 6-well plate. At 2 hpi, an agarose/DMEM overlay supplemented with rifampin (200 ng ml^{-1}) and spectinomycin (200 µg ml^{-1}) was added to infected cells as previously described[40] and the cells incubated for 14 days. Recombinant strains were isolated from 24 individual plaques and expanded in Vero cells. All recombinant strains were genotyped by PCR for the presence of CTL2M467 parental non-synonymous SNVs (Supplementary Table 3). Recombinant strain number 22 (M467 rs22) was found to harbour only the parental *cdu2-G607A* mutation (Cdu2-H203Y). *Chlamydia* strains were maintained as frozen stocks in SPG buffer.

***Chlamydia* growth assays.** HeLa and A549 cells were seeded in wells of two 96-well plates (input and output plates). Cells were infected with *Chlamydia* strains at an m.o.i. of 0.6. At 24 hpi, infected cells in the input plate were fixed with ice-cold methanol and stored in PBS. At 48 hpi, crude lysates in SPG were prepared from infected cells in output plates and a series of 1:10 dilutions were used to immediately infect corresponding HeLa or A549 cells seeded in wells of a 96-well plate. At 24 hpi, cells were fixed with ice-cold methanol. Fixed cells were stained with rabbit anti-Slc1[41] and Hoechst. Images from stained cells were captured on an EVOS cell imaging system (ThermoFisher scientific) with a 20X objective. Inclusion forming units (IFUs) were quantified using ImageJ (NIH). Output IFUs from each *Chlamydia* inoculum were normalized to their respective input IFUs. *Chlamydia* IFU production was measured from three independent biological replicates.

Visual and quantitative analysis of Golgi redistribution around *Chlamydia* inclusions. *Imaging.* HeLa and A549 cells grown on glass coverslips were infected with *Chlamydia* strains at m.o.i. of 0.8. At 26 hpi, cells were fixed with pre-warmed (37 °C) 3% formaldehyde in PBS for 20 min at room temperature. All washes and antibody stainings were performed with pre-warmed (37 °C) PBS and antibody solutions respectively. Fixed cells were stained with rabbit anti-Slc1[41] and mouse anti-GM130 antibodies (BD Biosciences), and Hoechst. Z-stacks of stained cells were captured on a Zeiss 880 inverted fluorescence microscope with a 63X objective (Zeiss).

Golgi redistribution quantification. For each Z-stack, maximum intensity Z-projections were generated with ImageJ (NIH). The length of Golgi (defined by GM130 staining) distributed around *Chlamydia* inclusions and the length of each inclusion perimeter (defined by Slc1 staining) were measured using the line tool from ImageJ (NIH). The ratio of Golgi length to inclusion perimeter length was determined, and values expressed as a percentage. Three independent experiments were performed to assess Golgi distribution. Golgi distribution was assessed from 6 fields for a total of 90 cells per independent experiment.

High-resolution imaging. Standard deviation Z-projections of captured images (see above) were generated and images minimally processed with ImageJ (NIH).

ChlaDUB expression in mammalian cells. *Imaging.* HeLa cells grown on glass coverslips were transfected with 1 µg of plasmid using Genejuice (EMD Millipore). At 23 h post transfection, cells were fixed with 4% paraformaldehyde, immunostained for GM130 (BD Biosciences 610822). Nucleic acids were stained with DAPI. Images were collected on a Nikon Eclipse Ti microscope with a Super Plan Fluor ELWD 40XC objective or a 3i Marianas spinning disk inverted confocal microscope with a 63X oil objective and a CMOS camera (Hamatsu). The images were then processed using SlideBook software and Photoshop CS4 Version 11.0 (Adobe).

Quantification of Golgi fragmentation. Images were converted from 16-bit to 8-bit binary using Fiji. Following selection of the region of interest, the number and surface area of Golgi-stained particles were quantified using the Analyze Particles tool of Fiji. A minimum of three independent experiments were performed to assess Golgi fragmentation, each consisting of ~65 counted cells. Multinucleated cells, as well as cells that were cycling through mitosis, were excluded from the analysis.

Western blotting. HeLa cells were transfected with 1 µg of plasmid using Genejuice (EMD Millipore). At 23 h post transfection, cells were lysed in RIPA buffer and the protein amount was assessed using the Pierce BCA Protein Assay Kit (Thermo). Then 20 µg of lysates were resolved by SDS–PAGE and transferred onto nitrocellulose. Membranes were blocked in 5% milk/TBST for 1 h and probed for GFP (sheep, 1:1,000, made in-house) and actin (rabbit, 1:10,000, Sigma A2266) for 1 h at room temperature. The IRDye 680LT Donkey anti-Rabbit IgG (LI-COR 926-68023) and IRDye 800CW Donkey anti-Goat IgG (cross-reacts with sheep IgG, LI-COR 926-32214) secondary antibodies were used at a concentration of 1:10,000 in 5% milk. Membranes were scanned using a LI-COR CLx Odyssey system and the Image Studio software, and minimally processed in Photoshop CS4 Version 11.0 (Adobe).

Statistical analyses. All statistical analyses were performed using GraphPad Prism 7.0. *Chlamydia* growth assays were analysed using a two-tailed Welch's *t*-test. All other analyses used a two-tailed Mann–Whitney *U*-test. All experiments contained three biological replicates. Data from these replicates are either combined or plotted separately, as described in the figure legends.

Reporting Summary. Further information on research design is available in the Nature Research Reporting Summary linked to this article.

Data availability

The data that support the findings in this study are available from the corresponding author on request. Coordinates and structure factors for the ChlaDUB1~Ub, ChlaDUB1~CoA and *C.a.* ChlaDUB structures have been deposited with the protein data bank, accession codes 6GZS, 6GZT and 6GZU respectively.

Received: 24 April 2018; Accepted: 13 September 2018;
Published online: 5 November 2018

References

1. Lin, Y. H. & Machner, M. P. Exploitation of the host cell ubiquitin machinery by microbial effector proteins. *J. Cell Sci.* **130**, 1985–1996 (2017).
2. Bastidas, R. J. & Valdivia, R. H. Emancipating Chlamydia: advances in the genetic manipulation of a recalcitrant pathogen. *Microbiol. Mol. Biol. Rev.* **80**, 411–427 (2016).
3. Rytkönen, A. et al. SseL, a *Salmonella* deubiquitinase required for macrophage killing and virulence. *Proc. Natl Acad. Sci. USA* **104**, 3502–3507 (2007).
4. Misaghi, S. et al. *Chlamydia trachomatis*-derived deubiquitinating enzymes in mammalian cells during infection. *Mol. Microbiol.* **61**, 142–150 (2006).
5. Catic, A., Misaghi, S., Korbel, G. A. & Ploegh, H. L. ElaD, a deubiquitinating protease expressed by *E. coli*. *PLoS ONE* **2**, e381 (2007).
6. Chosed, R. et al. Structural analysis of *Xanthomonas* XopD provides insights into substrate specificity of ubiquitin-like protein proteases. *J. Biol. Chem.* **282**, 6773–6782 (2007).
7. Mukherjee, S. et al. *Yersinia* YopJ acetylates and inhibits kinase activation by blocking phosphorylation. *Science* **312**, 1211–1214 (2006).
8. Mittal, R., Peak-Chew, S. Y. & McMahon, H. T. Acetylation of MEK2 and IκB kinase (IKK) activation loop residues by YopJ inhibits signaling. *Proc. Natl Acad. Sci. USA* **103**, 18574–18579 (2006).
9. Jones, R. M. et al. *Salmonella* AvrA coordinates suppression of host immune and apoptotic defenses via JNK pathway blockade. *Cell Host Microbe* **3**, 233–244 (2008).
10. Sheedlo, M. J. et al. Structural basis of substrate recognition by a bacterial deubiquitinase important for dynamics of phagosome ubiquitination. *Proc. Natl Acad. Sci. USA* **112**, 15090–15095 (2015).
11. Pruneda, J. N. et al. Molecular basis for ubiquitin and ubiquitin-like specificities in bacterial effector proteases. *Mol. Cell* **63**, 261–276 (2016).
12. Corn, J. E. & Vucic, D. Ubiquitin in inflammation: the right linkage makes all the difference. *Nat. Struct. Mol. Biol.* **21**, 297–300 (2014).
13. Le Negrate, G. et al. ChlaDub1 of *Chlamydia trachomatis* suppresses NF-kappaB activation and inhibitis IkappaBalpha ubiquitination and degradation. *Cell. Microbiol.* **10**, 1879–1892 (2008).
14. Mesquita, F. S. et al. The *Salmonella* deubiquitinase SseL inhibits selective autophagy of cytosolic aggregates. *PLoS Pathog.* **8**, e1002743 (2012).
15. Fischer, A. et al. *Chlamydia trachomatis*-containing vacuole serves as deubiquitination platform to stabilize Mcl-1 and to interfere with host defense. *eLife* **6**, e21465 (2017).
16. Zhang, Z. M. et al. Structure of a pathogen effector reveals the enzymatic mechanism of a novel acetyltransferase family. *Nat. Struct. Mol. Biol.* **23**, 847–852 (2016).
17. Mittal, R., Peak-Chew, S. Y., Sade, R. S., Vallis, Y. & McMahon, H. T. The acetyltransferase activity of the bacterial toxin YopJ of *Yersinia* is activated by eukaryotic host cell inositol hexakisphosphate. *J. Biol. Chem.* **285**, 19927–19934 (2010).
18. Reverter, D. & Lima, C. D. A basis for SUMO protease specificity provided by analysis of human senp2 and a senp2-SUMO complex. *Structure* **12**, 1519–1531 (2004).
19. Reverter, D. et al. Structure of a complex between NEDD8 and the Ulp/Senp protease family member Den1. *J. Mol. Biol.* **345**, 141–151 (2005).

20. Shen, L. et al. Structural basis of NEDD8 ubiquitin discrimination by the deNEDDylating enzyme NEDP1. *EMBO J.* **24**, 1341–1351 (2005).
21. Fullam, E. et al. Divergence of cofactor recognition across evolution: coenzyme A binding in a prokaryotic arylamine N-acetyltransferase. *J. Mol. Biol.* **375**, 178–191 (2008).
22. Sixt, B. S. & Valdivia, R. H. Molecular genetic analysis of *Chlamydia* species. *Annu. Rev. Microbiol.* **70**, 179–198 (2016).
23. Kokes, M. et al. Integrating chemical mutagenesis and whole-genome sequencing as a platform for forward and reverse genetic analysis of *Chlamydia*. *Cell Host Microbe* **17**, 716–725 (2015).
24. Heuer, D. et al. *Chlamydia* causes fragmentation of the Golgi compartment to ensure reproduction. *Nature* **457**, 731–735 (2009).
25. Dumoux, M. & Hayward, R. D. Membrane contact sites between pathogen-containing compartments and host organelles. *Biochim. Biophys. Acta, Mol. Cell Biol. Lipids* **1861**, 895–899 (2016).
26. Wang, X., Hybiske, K. & Stephens, R. S. Direct visualization of the expression and localization of chlamydial effector proteins within infected host cells. *Pathog. Dis.* **76**, fty011 (2018).
27. Henderson, B. An overview of protein moonlighting in bacterial infection. *Biochem. Soc. Trans.* **42**, 1720–1727 (2014).
28. Wesolowski, J. et al. *Chlamydia* hijacks ARF GTPases to coordinate microtubule posttranslational modifications and Golgi complex repositioning. *mBio* **8**, e02280–16 (2017).
29. Rejman Lipinski, A. et al. Rab6 and Rab11 regulate *Chlamydia trachomatis* development and golgin-84-dependent Golgi fragmentation. *PLoS Pathog.* **5**, e1000615 (2009).
30. Berrow, N. S. et al. A versatile ligation-independent cloning method suitable for high-throughput expression screening applications. *Nucleic Acids Res.* **35**, e45 (2007).
31. Schneider, C. A., Rasband, W. S. & Eliceiri, K. W. NIH Image to ImageJ: 25 years of image analysis. *Nat. Methods* **9**, 671–675 (2012).
32. Ekkebus, R. et al. On terminal alkynes that can react with active-site cysteine nucleophiles in proteases. *J. Am. Chem. Soc.* **135**, 2867–2870 (2013).
33. Kabsch, W. XDS. *Acta Crystallogr. D Biol. Crystallogr.* **66**, 125–132 (2010).
34. Evans, P. R. & Murshudov, G. N. How good are my data and what is the resolution?. *Acta Crystallogr. D Biol. Crystallogr.* **69**, 1204–1214 (2013).
35. Adams, P. D. et al. PHENIX: a comprehensive Python-based system for macromolecular structure solution. *Acta Crystallogr. D Biol. Crystallogr.* **66**, 213–221 (2010).
36. Terwilliger, T. C. et al. Decision-making in structure solution using Bayesian estimates of map quality: the PHENIX AutoSol wizard. *Acta Crystallogr. D Biol. Crystallogr.* **65**, 582–601 (2009).
37. Terwilliger, T. C. et al. Iterative model building, structure refinement and density modification with the PHENIX AutoBuild wizard. *Acta Crystallogr. D Biol. Crystallogr.* **64**, 61–69 (2008).
38. McCoy, A. J. et al. Phaser crystallographic software. *J. Appl. Crystallogr.* **40**, 658–674 (2007).
39. Emsley, P., Lohkamp, B., Scott, W. G. & Cowtan, K. Features and development of Coot. *Acta Crystallogr. D Biol. Crystallogr.* **66**, 486–501 (2010).
40. Nguyen, B. D. & Valdivia, R. H. Virulence determinants in the obligate intracellular pathogen *Chlamydia trachomatis* revealed by forward genetic approaches. *Proc. Natl Acad. Sci. USA* **109**, 1263–1268 (2012).
41. Chen, Y. S. et al. The *Chlamydia trachomatis* type III secretion chaperone Slc1 engages multiple early effectors, including TepP, a tyrosinephosphorylated protein required for the recruitment of CrkI-II to nascent inclusions and innate immune signaling. *PLoS Pathog.* **10**, e1003954 (2014).

Acknowledgements

We thank members of our laboratories for reagents and advice, particularly Lee Dolat (Duke University) for his contribution to some preliminary *Chlamydia* infection work. Access to DLS was supported in part by the EU FP7 infrastructure grant BIOSTRUCT-X (contract no. 283570). Work in the D.K. lab was funded by the Medical Research Council (grant no. U105192732), the European Research Council (grant no. 724804), and the Lister Institute for Preventive Medicine. J.N.P. was supported on an EMBO Long-Term Fellowship. Work in the R.H.V. lab was funded by the National Institute of Health (grant no. R01AI100759 to R.H.V.) and the National Institute of Allergy and Infectious Diseases (grant no. STI CRC U19 AI084044 to R.J.B. and R.H.V.). E.B. was supported by North West Cancer Research. B.S. was supported by the Medical Research Council.

Author contributions

Conceptualization was by J.N.P. and D.K. The investigation was carried out by J.N.P., R.J.B., E.B., K.N.S. and B.S. The methodology was done by R.J.B., R.H.V., M.J.C. and S.U. The writing was by J.N.P. and D.K. Funding acquisition was by D.K., R.H.V., R.J.B., S.U. and M.J.C.

Competing interests

The authors declare no competing interests.

Additional information

Supplementary information is available for this paper at https://doi.org/10.1038/s41564-018-0271-y.

Reprints and permissions information is available at www.nature.com/reprints.

Correspondence and requests for materials should be addressed to D.K.

Publisher's note: Springer Nature remains neutral with regard to jurisdictional claims in published maps and institutional affiliations.

nature research

Corresponding author(s): David Komander

☐ Initial submission ☐ Revised version ☒ Final submission

Life Sciences Reporting Summary

Nature Research wishes to improve the reproducibility of the work that we publish. This form is intended for publication with all accepted life science papers and provides structure for consistency and transparency in reporting. Every life science submission will use this form; some list items might not apply to an individual manuscript, but all fields must be completed for clarity.

For further information on the points included in this form, see Reporting Life Sciences Research. For further information on Nature Research policies, including our data availability policy, see Authors & Referees and the Editorial Policy Checklist.

Experimental design

1. Sample size

Describe how sample size was determined.

Sample size was not predetermined, but standardised during analysis to improve comparisons across groups (see below). Sample sizes were set to a minimum value (as described in the figure and methods) after which the inclusion of additional data had no affect on median values.

2. Data exclusions

Describe any data exclusions.

Biological data sets were set to a consistent number of data points in an unbiased fashion to normalise statistical power across groups. Exclusion parameters were not predetermined, but applied randomly such that median values were not affected.

3. Replication

Describe whether the experimental findings were reliably reproduced.

All attempts at replication were successful, and data from replicate experiments are shown where appropriate.

4. Randomization

Describe how samples/organisms/participants were allocated into experimental groups.

Randomization was not required in our study as all of our experiments are highly controlled and quantitative.

5. Blinding

Describe whether the investigators were blinded to group allocation during data collection and/or analysis.

Images used for the quantification of Golgi fragmentation following Chlamydia infection were blinded prior to analysis.

Note: all studies involving animals and/or human research participants must disclose whether blinding and randomization were used.

6. Statistical parameters

For all figures and tables that use statistical methods, confirm that the following items are present in relevant figure legends (or in the Methods section if additional space is needed).

n/a	Confirmed
☐	☒ The exact sample size (*n*) for each experimental group/condition, given as a discrete number and unit of measurement (animals, litters, cultures, etc.)
☐	☒ A description of how samples were collected, noting whether measurements were taken from distinct samples or whether the same sample was measured repeatedly
☐	☒ A statement indicating how many times each experiment was replicated
☐	☒ The statistical test(s) used and whether they are one- or two-sided (note: only common tests should be described solely by name; more complex techniques should be described in the Methods section)
☐	☒ A description of any assumptions or corrections, such as an adjustment for multiple comparisons
☐	☒ The test results (e.g. *P* values) given as exact values whenever possible and with confidence intervals noted
☐	☒ A clear description of statistics including central tendency (e.g. median, mean) and variation (e.g. standard deviation, interquartile range)
☒	☐ Clearly defined error bars

See the web collection on statistics for biologists for further resources and guidance.

Software

Policy information about availability of computer code

7. Software

Describe the software used to analyze the data in this study.	XDS (Jan 10, 2014), CCP4i (2.2.1), Aimless (0.3.11), Phenix (1.8.2), Phaser (2.5.3), Coot (0.6.2), PyMol (1.8.4.2), Slidebook (v6), Fiji (1.0), and Photoshop (CS4).

For manuscripts utilizing custom algorithms or software that are central to the paper but not yet described in the published literature, software must be made available to editors and reviewers upon request. We strongly encourage code deposition in a community repository (e.g. GitHub). *Nature Methods* guidance for providing algorithms and software for publication provides further information on this topic.

Materials and reagents

Policy information about availability of materials

8. Materials availability

Indicate whether there are restrictions on availability of unique materials or if these materials are only available for distribution by a for-profit company.	All unique materials are available from the authors.

9. Antibodies

Describe the antibodies used and how they were validated for use in the system under study (i.e. assay and species).	Mouse anti-GM130: BD Biosciences 610822 (clone 35/GM130 (RUO)). Validated by BD Biosciences. 1:100 dilution for IF. Rabbit anti-Slc1: Generated in-house and validated previously (see reference 41). 1:400 dilution for IF. Sheep anti-GFP: Generated in-house and validated on recombinant protein. 1:1000 dilution for Western blot. Rabbit anti-Actin: Sigma A2266 (polyclonal). Validated by Sigma. 1:10,000 dilution for Western blot. IRDye 680LT Donkey anti-Rabbit: LI-COR 926-68023. Validated by LI-COR. 1:10,000 dilution for Western blot. IRDye 800CW Donkey anti-Goat: LI-COR 926-32214. Validated by LI-COR. 1:10,000 dilution for Western blot.

10. Eukaryotic cell lines

a. State the source of each eukaryotic cell line used.	All cell lines were sourced from ATCC.
b. Describe the method of cell line authentication used.	ATCC authenticates its cell lines through morphology, karyotyping, and STR analyses.
c. Report whether the cell lines were tested for mycoplasma contamination.	All cell lines were routinely tested with PCR screening and confirmed negative for mycoplasma contamination.
d. If any of the cell lines used are listed in the database of commonly misidentified cell lines maintained by ICLAC, provide a scientific rationale for their use.	None of the cell lines used are listed in the ICLAC database of commonly misidentified cell lines.

Animals and human research participants

Policy information about studies involving animals; when reporting animal research, follow the ARRIVE guidelines

11. Description of research animals

Provide details on animals and/or animal-derived materials used in the study.	No animals were used in this study.

Policy information about studies involving human research participants

12. Description of human research participants

Describe the covariate-relevant population characteristics of the human research participants.	This study did not involve human research participants.